Pyrrolo[1,4]benzodiazepine Antitumor Antibiotics: Evidence for Two Forms of Tomaymycin Bound to DNA†

Mary D. Barkley*,‡
Department of Biochemistry, University of Kentucky Medical Center, Lexington, Kentucky 40536
Steve Cheatham, David E. Thurston, and Laurence H. Hurley*
Drug Dynamics Institute, College of Pharmacy, University of Texas at Austin, Austin, Texas 78712
Received May 15, 1985; Revised Manuscript Received December 13, 1985

ABSTRACT: Tomaymycin is an antibiotic belonging to the pyrrolo[1,4]benzodiazepine group of antitumor compounds. Previous studies have shown that tomaymycin and other members of this group, which include anthramycin, sibiromycin, and the neothramycins, bind covalently through N-2 of guanine and lie within the minor groove of DNA. Two fluorescent ground-state species of tomaymycin were observed in protic solvents and on DNA. ^{1}H NMR studies showed that the two fluorescent species in methanol are the 11*R*,11a*S* and 11*S*,11a*S* diastereomeric 11-methyl ethers of tomaymycin. On the basis of epimerization experiments and exchange of carbon-13 from $^{13}CH_3OH$ into the C-11 methoxy group of the tomaymycin methyl ether, a mechanism is proposed for their interconversion via 10,11-anhydrotomaymycin. Coupling information revealed that the solution conformations of the two diastereomers differ, with the C-5 carbonyl lying closer to the plane of the aromatic ring in the 11*R*,11a*S* diastereomer. The fluorescence excitation and emission spectra of the two emitting species in methanol were separated by time-resolved fluorescence spectroscopy and were associated with the diastereomeric forms identified by ^{1}H NMR. Time-resolved fluorescence studies of tomaymycin in protic solvents and on DNA indicated that the absorption spectrum of the longer lifetime component (11*R*,11a*S* form) is red-shifted relative to the absorption spectrum of the shorter lifetime component (11*S*,11a*S* form), consistent with more extensive conjugation. The two conformational forms of tomaymycin on DNA were tentatively identified as the 11*S*,11a*S* and 11*R*,11a*S* diastereomeric adducts, which bind in opposite orientations in the minor groove. This proposal is supported by molecular modeling studies using a 6-mer duplex adduct of $d(ATGCAT)_2$.

Tomaymycin is an antitumor antibiotic produced by *Streptomyces tomaymyceticus* that belongs to the P[1,4]B[1] group of antibiotics (Arima et al., 1972; Hurley & Thurston, 1984). Other examples of P[1,4]B antibiotics include anthramycin, sibiromycin, and the neothramycins A and B. The structure of tomaymycin 11-methyl ether (see Figure 1) was elucidated by chemical and spectroscopic means (Kariyone et al., 1971), an X-ray structure has been published (Arora, 1981), and a total synthesis has been reported (Tozuka et al., 1983). The potent antitumor activity of the P[1,4]B antibiotics is believed to be due to their ability to bind covalently to DNA (Hurley et al., 1977). In the case of anthramycin it has been conclusively demonstrated by ^{1}H and ^{13}C NMR that the carbinolamine (or its chemical equivalent) reacts with the exocyclic amino group of guanine to form an aminal linkage (Graves et al., 1984) (see Scheme I). Primarily on the basis of circumstantial evidence, CPK models of the P[1,4]B antibiotic–DNA adducts have been proposed (Hurley & Petrusek, 1979; Petrusek et al., 1981). The CPK models and molecular graphics studies show that the nucleus of all of the P[1,4]B drug molecules resides completely within the minor groove of DNA, without apparent distortion of the DNA. Structure–activity relationships that support these models for the binding of tomaymycin and related antibiotics to DNA have been published (Thurston & Hurley, 1984). Reviews on the biosynthesis (Hurley, 1980), mechanism of action, and pharmacological activity of tomaymycin and other agents in this group have appeared (Hurley, 1977).

Scheme I: Reaction of P[1,4]B's with DNA

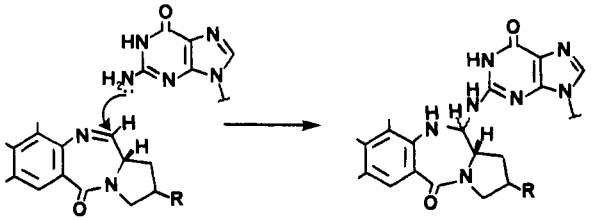

Although tomaymycin, like other members of the P[1,4]B's, is believed to bind covalently through C-11 of the drug molecule to N-2 of guanine, several lines of evidence suggest that it does not have complete overlap of DNA binding sites with anthramycin. For example, there is incomplete competition for binding sites on DNA between anthramycin and tomaymycin (Hurley et al., 1977), and recent investigations on the sequence specificity of the P[1,4]B's confirm the partial overlap of binding sequences (Hertzberg et al., 1986). Our observation that there are two fluorescent species of tomaymycin in solution and the DNA adduct has provided an op-

†This work was supported by U.S. Public Health Service Grants CA-31232, CA-35813, and GM-22873 and the Welch Foundation.
‡Present address: Department of Chemistry, Louisiana State University, Baton Rouge, LA 70803.

[1] Abbreviations: CPK, Corey, Pauling, and Koltun; TME, tomaymycin 11-methyl ether; MTME, 8-*O*-methyltomaymycin 11-methyl ether; P[1,4]B, pyrrolo[1,4]benzodiazepine; POPOP, *p*-bis[2-(5-phenyloxazolyl)]benzene; 1-D, one dimensional; 2-D, two dimensional; HPLC, high-performance liquid chromatography; RP-TLC, reverse-phase thin-layer chromatography; MS, mass spectroscopy; EDTA, ethylenediaminetetraacetic acid; fwhm, full width at half-maximum; ex, excitation; em, emission; Pu, purine; Py, pyrimidine.

0006-2960/86/0425-3021$01.50/0

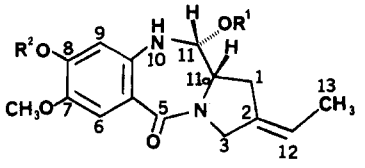

TOMAYMYCIN	$R^1=R^2=H$
TME	$R^1=CH_3;R^2=H$
MTME	$R^1=R^2=CH_3$

FIGURE 1: Structures of tomaymycin and related compounds.

portunity to probe the apparent heterogeneity of tomaymycin binding to DNA in more detail. In this paper, we show that there are two ground-state forms of tomaymycin in protic but not aprotic solvents, corresponding to epimers at the reactive C-11. The diastereomers were identified and their solution conformations were determined by 1-D and 2-D ^1H NMR. The two diastereomers were associated with their respective absorption and emission spectra and excited-state lifetimes by time-resolved fluorescence spectroscopy. By analogy with the results in solution, we propose that the two fluorescent species bound to DNA may represent two diastereomeric DNA adducts. Finally, we present molecular modeling studies to suggest how the different diastereomers of tomaymycin bind to DNA.

Materials and Methods

Chemicals. TME was a generous gift from Dr. Kohsaka of Fujisawa Pharmaceuticals (Japan). MTME and 10,11-anhydrotomaymycin were prepared as described below from TME. Other chemicals were obtained from commercial sources.

MTME. TME (5 mg) was dissolved in 1 mL of HPLC-grade methanol (Fisher), and excess ethereal diazomethane was added. Reaction progress was monitored by RP-TLC using 70% MeOH/H_2O as solvent. After 30 min, quantitative conversion of the TME (R_f = 0.59) to MTME (R_f = 0.49) had occurred. The solvent was removed in vacuo to afford 5.8 mg of crystalline product. Analytical data (^1H NMR, IR, MS) are consistent with the structure.

10,11-Anhydrotomaymycin. 10,11-Anhydrotomaymycin was prepared by dissolving TME in chloroform as previously described (Tozuka et al., 1983).

The purity of antibiotic samples was evaluated by reverse-phase HPLC (Waters Associates μBondapack C_{18}; 70% MeOH/H_2O). Retention times were 10.8 min for TME and 16.1 min for MTME. As estimated by peak areas, the MTME sample contained minor impurities totaling approximately 4% and was used directly; the TME sample contained approximately 2% impurities.

$CDCl_3$, CD_3CN, and CD_3OD for NMR studies were "100% atom D", purchased from Aldrich Chemical Co., and $^{13}CH_3OH$ was 99 atom %, purchased from Sigma Chemical Co. HPLC-grade solvents were used for optical studies. Chloroform (without 1% ethanol) was purchased from Burdick and Jackson. Buffer is 1 mM cacodylic acid (Sigma), 0.1 M NaCl, and 0.15 mM EDTA, adjusted to the desired pH with NaOH. Calf thymus DNA (Sigma type I) was purified by phenol extraction and dialyzed against pH 6.4 buffer. DNA concentration was determined from the absorbance at 260 nm by using the extinction coefficient 6.8×10^3 M^{-1} cm^{-1}.

NMR Studies. All ^1H NMR spectra were recorded on a Nicolet NT-200 or GE-Nicolet 360 or 500 spectrometer with tetramethylsilane (TMS) as an internal standard. Spectra observed in CD_3OD were taken on 3-mg samples examined 72 h after dissolving crystalline (11*R*,11a*S*)-TME in solvent, unless stated otherwise. Saturated solutions of tomaymycin were run in CDCN and $CDCl_3$ because of low solubility in these solvents. Carbon NMR spectra were recorded at 90 MHz on a GE-Nicolet 360 spectrometer. TME (20 mg) was equilibrated with either CH_3OH or $^{13}CH_3OH$, and the solvent was removed by using a stream of argon. The residues were dissolved in Me_2SO-d_6, and TMS was added as an internal standard.

Fluorescence Studies. (*1*) *Antibiotic Solutions.* Solutions of antibiotics were usually prepared from methanol stock solutions stored at −20 °C. The concentration of TME stock solution was determined from the absorbance at 320 nm by using the extinction coefficient 3.6×10^3 M^{-1} cm^{-1} (Arima et al., 1972). The concentration of MTME stock solution was determined by weight. An aliquot of the stock solution was placed in a vial, and the methanol was evaporated under vacuum or by a stream of N_2. Solvent was added to give the desired final concentration. Antibiotic solutions in protic solvents were equilibrated overnight at room temperature prior to use. DNA adducts were prepared by adding calf thymus DNA solution (2.7×10^{-3} M nucleotide in pH 6.4 buffer) to give a phosphate/drug ratio of 125. The reaction was allowed to equilibrate for 2 days at 4 °C. This solution was diluted 2-fold with pH 6.4 buffer for steady-state fluorescence measurements. The antibiotics were stable in protic solvents for several weeks at room temperature and for longer periods at 4 °C. DNA adducts showed no changes with storage at 4 °C for at least 1 month. Antibiotic solutions in acetonitrile were prepared by dilution of acetonitrile stock solutions stored at −20 °C. The antibiotics have limited stability in acetonitrile, as was apparent from progressive changes in the absorption spectra: the long wavelength band was gradually displaced by absorbance in the ultraviolet. However, no changes were noted in fluorescence spectra or lifetime. Presumably the absorption spectral changes are due to conversion of the methyl ether to the nonfluorescent imine and subsequent degradation. A dilute solution prepared directly from crystalline TME also showed evidence of decomposition. Fresh dilutions of acetonitrile stock solution gave reproducible absorption spectra which usually did not change over 1–2 days at room temperature.

Samples were placed in 1-cm stoppered cuvettes and thermostated at 25 °C in all experiments. The absorbance of solutions was <0.1 at the long-wavelength maximum. The total absorbance of DNA-containing solutions was <0.1 at all excitation wavelengths. Absorbance was measured by using a Cary 118 spectrophotometer.

(*2*) *Steady-State Measurements.* Steady-state fluorescence was measured by using a SPEX Fluorolog 211 photon-counting spectrofluorometer, controlled through a Datamate terminal. All spectra were acquired in the ratio mode with 3.6-nm excitation band-pass, 7.2-nm emisson band-pass, and Glans polarizers set at the magic angle (excitation vertical, emission 54.7° to the vertical). Background fluorescence from a solvent blank was subtracted, and the spectra were corrected for wavelength-dependent instrumental factors. The excitation correction was determined with a rhodamine quantum counter placed in the sample compartment by using the absorbance accessory. The emission correction was supplied by the factory.

Fluorescence quantum yields were determined relative to quinine sulfate. Fresh solutions of quinine bisulfate (Eastman Kodak) were prepared weekly by dissolving a few crystals in 1 N H_2SO_4 (double distilled, GFS Chemicals) and adjusting

the absorbance to <0.1 at the long-wavelength maximum. Sample quantum yields were calculated by using $\phi = 0.546$ for quinine sulfate (Melhuish, 1961). Since the refractive indices of methanol, water, and acetonitrile are very similar, the refractive index correction was not applied. Errors in quantum yields are about 5%.

(*3*) *Time-Resolved Measurements.* Fluorescence decay measurements were made in a Photochemical Research Associates nanosecond fluorometer interfaced to a Digital Equipment Corporation MINC-11 computer. The flash lamp was filled with 1.7 atm of N_2 and operated at 30 kHz with about 5 kV applied across a 1.5–2-mm electrode gap. Under these conditions the pulse width was 1.5–1.7 ns fwhm. Excitation wavelength was selected by an interference filter (12-nm band-pass), and emission wavelength was selected by a monochromator (10-nm band-pass). The following interference filters were used: microCoatings, Inc., 313; Corion 337, 350. Since the incident light is unpolarized, a dichroic film polarizer oriented at 35.2° to the vertical was placed on the emission side to correct for anisotropic effects. Fluorescence decays from a sample and a reference fluorophore were acquired contemporaneously to about 2×10^4 counts in the peak. The counting rate was <2% of the lamp repetition rate. Decay curves were stored in 512 channels, with 0.109 ns/channel. A solution of POPOP (Fluka) in aqueous ethanol and 0.5 M KI (containing a trace of sodium thiosulfate to retard I_3^- formation) was used as reference fluorophore. A lifetime of 0.33 ± 0.02 ns for the quenched POPOP was determined in separate experiments with a monoexponential standard (anthracene in ethanol).

Fluorescence decay data were deconvolved by using the reference decay instead of a lamp profile in a modified least-squares analysis (Kolber & Barkley, 1986) based on the Marquardt algorithm (Bevington, 1969). Goodness of fit was judged by the magnitude of reduced χ_r^2 and the shape of the autocorrelation function of the weighted residuals. The data were fitted to a sum of exponentials:

$$i(\lambda_{ex},\lambda_{em};t) = \sum_i \alpha_i(\lambda_{ex},\lambda_{em}) \exp(-t/\tau_i)$$

with amplitudes α_i and lifetimes τ_i. Decay curves measured for a sample at various excitation and emission wavelengths were analyzed by a global program (Knutson et al., 1983), with the constraint that the lifetimes τ_i are independent of wavelength. Our global program deconvolves up to 12 decay curves simultaneously for up to 3 exponentials, using a fixed or variable lifetime for the reference decay. The validity of assumed models for the fluorescence decay was tested by single-curve analysis, multiple-curve analysis with the reference lifetime variable, and multiple-curve analysis with the reference lifetime fixed. The error in fluorescence lifetimes in repeated experiments was about 5–10%.

The decay-associated spectra were derived by combining data from time-resolved and steady-state fluorescence experiments. Decay-associated emission spectra $I_i(\lambda_{em})$ were calculated from the time-resolved emission spectral data scaled to the corrected steady-state emission spectrum $I(\lambda_{em})$ at the same excitation wavelength:

$$I_i(\lambda_{em}) = I(\lambda_{em})\alpha_i(\lambda_{em})\tau_i / \sum_i \alpha_i(\lambda_{em})\tau_i$$

Decay-associated excitation spectra were obtained by an indirect method kindly provided by Dr. J. R. Knutson, which involves solving a set of simultaneous equations. For TME in methanol the equations were generated by combining corrected steady-state excitation spectra at 380- and 430-nm emission wavelengths with time-resolved data at 313-nm excitation wavelength and the same emission wavelengths. The amplitudes α_i of the fluorescence decays used in these equations were scaled to the corrected steady-state emission spectrum at 313-nm excitation.

Epimerization Studies. The epimerization of TME in methanol was monitored by ^{1}H NMR, absorbance, and fluorescence lifetime measurements. Crystalline TME was dissolved in CD_3OD, and ^{1}H NMR spectra were recorded at 0.5, 1.25, and 2.0 h. The relative amounts of the two enantiomers were determined by integration of their respective H-6 and H-9 protons. A delay of 10 s was inserted between pulses to minimize integration errors due to incomplete relaxation. For absorbance and fluorescence measurements, a few crystals of TME were dissolved in several milliliters of methanol, the absorbance was adjusted to about 0.1 at the long-wavelength maximum, and the final solution was put in two cuvettes. The absorption spectrum and the fluorescence decay at λ_{ex} = 313 nm and λ_{em} = 405 nm were measured at 45-min intervals for about 10 h, beginning 30 min after adding the crystals. At the end of the experiment, decay curves were acquired at λ_{em} = 380–430 nm (10-nm increments) for λ_{ex} at both 313 and 337 nm. The fluorescence decay curves for the equilibrated solution were devonvolved by global analysis, and the lifetimes were used in single-curve analyses to recover the amplitudes at various times.

Molecular Graphics Studies. Molecular graphics studies were carried out by Dr. William A. Remers while he was on sabbatical leave at Searle Laboratories. For complete details on energy minimization calculations, see Remers et al. (1986).

Results

^{1}H NMR and Fluorescence of Tomaymycin in Aprotic Solvents. The crystalline form of TME is the 11*R*,11a*S* diastereomer (Arora, 1981), and when the crystals are dissolved in polar aprotic solvents, such as acetonitrile or Me_2SO, one fluorescent ground-state species is observed. The partial ^{1}H NMR of TME in CD_3CN is shown in Figure 2A. A similar ^{1}H NMR spectrum of TME in Me_2SO was assigned to the 11*R*,11a*S* diastereomer (Tozuka & Takaya, 1983). The absorption spectrum of TME in acetonitrile is similar to that in methanol (Arima et al., 1972) with long-wavelength maximum at about 320 nm (Table I). The fluorescence emission spectrum has a maximum at about 380 nm. The excitation and emission spectra are independent of emission and excitation wavelength (not shown). The fluorescence decay gives a reasonable fit (χ_r^2 = 1.7) to a single exponential with lifetime of 1.8 ns (Table II). The fit is improved (χ_r^2 = 1.1) by including a second exponential with negative amplitude and very short decay time. A negative term in a fluorescence decay indicates an excited-state reaction, which has not been investigated further.

In chloroform, tomaymycin is rapidly converted to 10,11-anhydrotomaymycin. This species was previously identified as an imine by ^{1}H NMR (Tozuka et al., 1983), on the basis of the characteristic doublet found at δ 7.67 (J = 4.2 Hz). The absorption spectrum of the imine shows a substantial change in the chromophore. The long-wavelength absorption band is replaced by a broad featureless shoulder extending into the ultraviolet (not shown). The species in chloroform is nonfluorescent.

^{1}H NMR and Fluorescence of Tomaymycin in Methanol. (*1*) *^{1}H NMR Studies.* In protic solvents such as alcohols and aqueous buffers, tomaymycin occurs in two fluorescent ground-state forms. The two forms are apparent in the ^{1}H NMR of TME after equilibration in CD_3OD. As seen in Figure 2B, the H-11 protons of the two forms resonate between

Table I: Spectral Data for TME, MTME, Tomaymycin, and 8-*O*-Methyltomaymycin

		absorbance		fluorescence		
solvent	compd	λ_{max} (nm)	$\epsilon_{max} \times 10^{-3}$ (M^{-1} cm^{-1})	λ_{ex} (nm)	λ_{em}^{max} (nm)	ϕ(app)
MeOH	TME	319	3.6	296	402	0.31
				320	400	0.34
				342	398	0.55
	MTME	320	3.7	296	405	0.33
				320	403	0.37
				342	401	0.60
buffer, pH 5.1	tomaymycin	309	3.4	285	413	0.068
				308	411	0.075
				333	410	0.096
	8-*O*-methyltomaymycin	309	3.7	285	413	0.072
				308	413	0.087
				333	412	0.11
MeCN[a]	TME	319	3.8	298	377	
				320	376	0.13
				337	377	
	MTME	319	3.9	298	383	
				320	383	0.18
				337	383	
calf thymus DNA	tomaymycin	331	3.4	310	406	0.23
				330	407	0.31
				350	408	0.37
	8-*O*-methyltomaymycin	330	3.6	310	408	0.29
				330	407	0.40
				350	407	0.52

[a] Absorbance and thus quantum yield measurements are approximate due to the presence of nonfluorescent species. See Materials and Methods.

Table II: Fluorescence Decay Data for TME, MTME, Tomaymycin, and 8-*O*-Methyltomaymycin[a]

solvent	compd	λ_{ex} (nm)	λ_{em} (nm)[b]	α_1[c]	τ_1 (ns)	α_2	τ_2 (ns)
MeOH	TME	313	400	0.32	3.3	0.68	4.9
		337	400	0.15		0.85	
	MTME	313	400	0.17	2.7	0.86	5.4
		337	400	0.04		0.96	
buffer, pH 5.1	tomaymycin	313	410	0.999	1.1	0.001	10
	8-*O*-methyltomaymycin	313	410	0.99	1.3	0.01	8
		337	410	0.98		0.02	
MeCN	TME	313		1.00	1.8		
		337		1.00			
	MTME	313		1.00	2.3		
		337		1.00			
calf thymus DNA	tomaymycin	313		0.37	3.0	0.63	5.5
		337		0.34		0.66	
		355		0.30		0.70	
	8-*O*-methyltomaymycin	313		0.39	4.2	0.61	6.8
		355		0.32		0.68	

[a] Decay parameters were obtained by global analysis of up to 12 decay curves measured at the indicated excitation wavelength(s) and several emission wavelengths. [b] No entry in this column means that the amplitudes are independent of emission wavelength. [c] Fractional amplitudes; $\sum \alpha_i = 1$.

4.20 and 4.70, ppm, whereas the aromatic H-6 and H-9 protons resonate between 6.20 and 7.40 ppm. Integration of these resonance signals indicates that the two species are present in approximate proportions of 65:35. In contrast, the ^{1}H NMR of TME in methanol taken immediately after dissolving the crystalline sample shows only one species (Figure 2C), which corresponds to the form found in acetonitrile (Figure 2A). The ^{1}H NMR of 10,11-anhydrotomaymycin was also examined immediately after dissolution in methanol. This spectrum (Figure 2D) indicates that the imine has converted to the two forms of TME present in methanol, with a greater proportion of the species corresponding to the one present in lesser concentration at equilibrium (compare to Figure 2B). However, if this sample is allowed to equilibrate, a spectrum identical with the spectrum of TME equilibrated in methanol (Figure 2B) is obtained.

Although the species of tomaymycin in aprotic solvents have been identified previously by ^{1}H NMR (Tozuka & Takaya, 1983; Tozuka et al., 1983), the equilibrium mixture in methanol has not been reported. Conceivably, the two forms in protic solvents could be due to proton transfer, tautomers, conformers, or epimers at C-11. To test whether proton transfer or tautomerism might be responsible for the equilibrium mixture in methanol, the 8-*O*-methyl derivative (MTME) of TME was prepared. This derivative lacks the 8-phenolic proton of tomaymycin likely to participate in proton transfer to solvent or tautomerism with the C-5 carbonyl. Both possibilities are excluded by the ^{1}H NMR, which still shows two species in methanol (Figure 2E). If the two species in methanol represent two conformers of the drug molecule in protic solvents, then the ^{1}H NMR signals of the two forms should begin to coalesce at elevated temperatures. However, heating the equilibrated sample of TME in methanol to 65 °C did not simplify the ^{1}H NMR spectrum (not shown), eliminating the possibility that the doubling of the proton signals in methanol is due to different conformational forms. A fourth and more likely possibility was epimerization at the C-11 position, a phenomenon first observed by Leimgruber

Scheme II: Proposed Mechanism for Epimerization at C-11 of Tomaymycin via 10,11-Anhydrotomaymycin

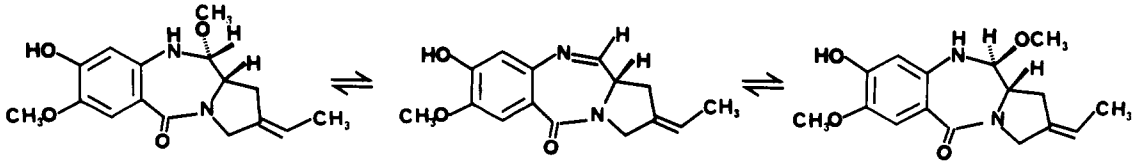

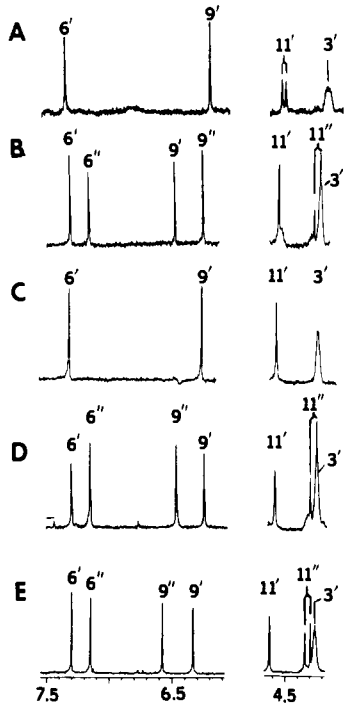

FIGURE 2: Partial ^1H NMR spectra of TME, 10,11-anhydrotomaymycin, and MTME in various solvents: (A) TME in acetonitrile; (B) TME in methanol after 72 h; (C) TME in methanol immediately after dissolution; (D) 10,11-anhydrotomaymycin in methanol immediately after dissolution; (E) MTME in methanol after 72 h.

et al. (1965) for anthramycin. Since the crystalline form of TME is known to be the 11*R*,11a*S* diastereomer (Arora, 1981), the single species found in acetonitrile and also the predominance of the same species found immediately after dissolution in methanol are easily rationalized. Upon standing in methanol, the 11*R*,11a*S* diastereomer then equilibrates to a mixture of the two diastereomeric forms (11*S*,11a*S* and 11*R*,11a*S*), probably by conversion via the imine 10,11-anhydrotomaymycin (Scheme II).[2] Finally, addition of methanol to 10,11-anhydrotomaymycin preferentially gives rise to the 11*S*,11a*S* diastereomer. This presumably reflects a sterically favored approach of methanol to one face of the molecule. The initial mixture is slowly converted to the same equilibrium mixture of the two diastereomeric forms found when the crystalline form (11*R*,11a*S*) is dissolved and equilibrated. In summary, we suggest that the two fluorescent ground-state forms of tomaymycin in methanol occur by epimerization at the C-11 position, which proceeds by way of attack by methanol of the intermediate 10,11-anhydrotomaymycin (Scheme II). In order to verify this interpretation, a ^{13}C NMR experiment using $^{13}CH_3OH$ as the solvent for the equilibration was carried out. A comparison of the partial ^{13}C NMR spectra of TME equilibrated in $^{13}CH_3OH$ or CH_3OH prior to dissolution in Me_2SO is shown in panels A and B,

[2] The alternative explanation is an S_N1 or S_N2 type displacement at C-11. However, given the existence of the imine, we favor the mechanism shown in Scheme I.

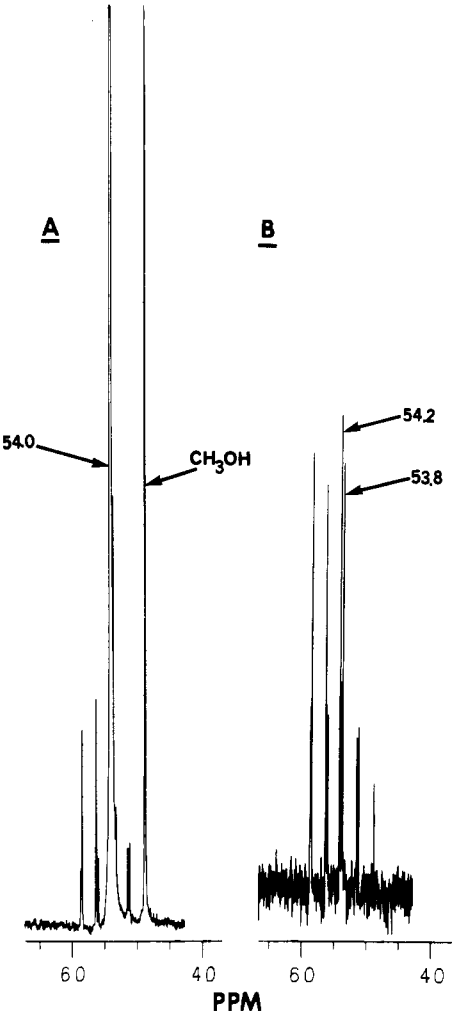

FIGURE 3: Partial ^{13}C NMR spectra of TME in Me_2SO-d_6 after preequilibriation in (A) $^{13}CH_3OH$ and (B) CH_3OH.

respectively, of Figure 3. Whereas the sample preequilibriated in CH_3OH (Figure 3B) shows resonance signals at 53.8 and 54.2 ppm that are assigned to the two C-11 methoxy carbons present at natural abundance, the $^{13}CH_3OH$-preequilibrated sample shows a highly enriched carbon-13 resonance signal at 54.0 ppm (Figure 3A). Integration of the resonance signal at 54.0 ppm in Figure 3A relative to the equivalent signals at 53.8 and 54.2 ppm in Figure 3B shows complete exchange of the C-11 methoxy carbons with $^{13}CH_3OH$. These results are consistent with the mechanism proposed in Scheme II.

The conformations of the 11*R*,11a*S* and 11*S*,11a*S* diastereomers were analyzed by using the Karplus rule (Karplus, 1959). The chemical shift and coupling information obtained from a 360-MHz ^1H NMR of the two diastereomers of TME in methanol are given in Table III. A 2-D homonuclear *J*-correlated (COSY) experiment on the equilibrated mixture confirmed all the proton assignments and identified the coupled spin systems (not shown). Considering the coupling constants (Table III) together with the previously published data in Me_2SO-d_6 (Tozuka & Takaya, 1983), the conformation of the 11*R*,11a*S* diastereomer in CD_3OD appears identical with the

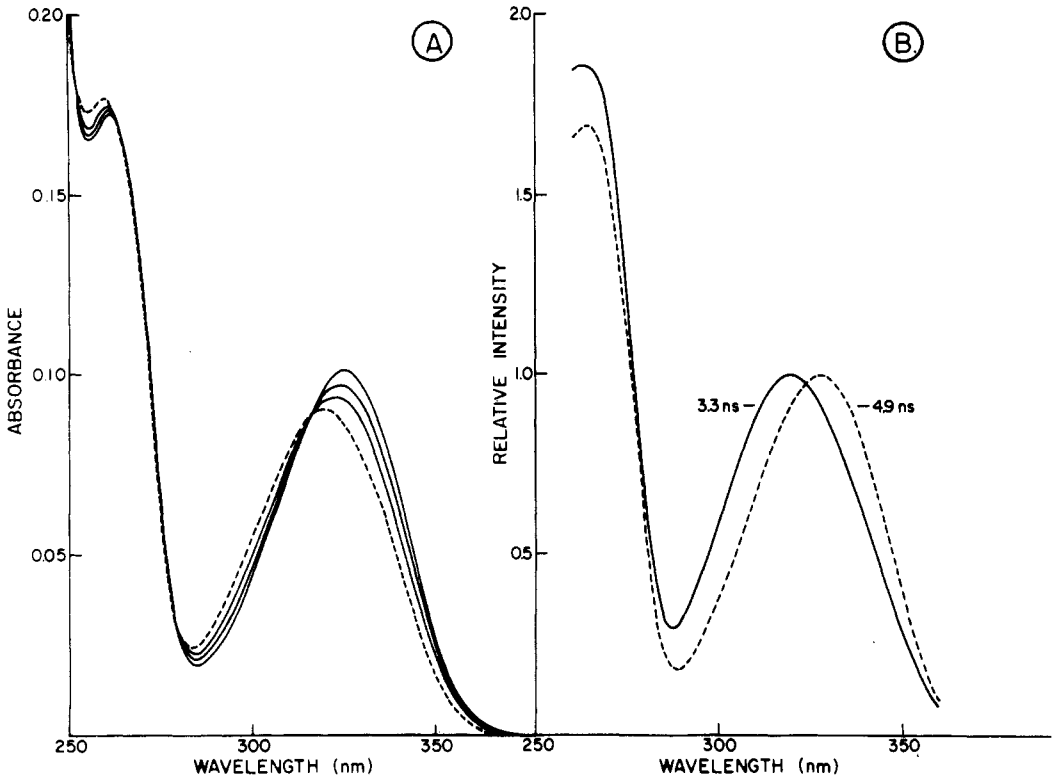

FIGURE 4: Absorption and fluorescence excitation spectra of TME in methanol. (A) Absorption spectra at various times after adding crystals to methanol: (—, upper curve) 0.5 h; (—, middle curve) 1.25 h; (—, lower curve) 2.0 h; (---) equilibrium. Isosbestic points are at 316, 279, and 263 nm. (B) Decay-associated excitation spectra: (—) 3.3-ns component; (---) 4.9-ns component. Spectra are normalized to the long-wavelength peak.

Table III: 360-MHz Spectrum of TME Diastereomers at Equilibrium in Methanol (CD_3OD)

	(11*R*,11a*S*)-TME		(11*S*,11a*S*)-TME	
proton[a]	chemical shift[b] (ppm)	mult[c] and J_{H-H} (Hz)	chemical shift (ppm)	mult and J_{H-H} (Hz)
1-Ha	2.97	dd; 15.3, 10.8	2.75	dd; 14.6, 10.0
1-Hb	2.69	bd; 15.3	2.63	bd; 14.6
3-Ha	4.25	bs	4.06	d; 14.6
3-Hb[d]				
6-H	7.28	s	7.13	s
9-H	6.22	s	6.43	s
11-H	4.58	s	4.27	d; 10.4
11a-H	3.96	dd; 10.8, 4.6	3.72	td; 10.4, 3.5
12-H	5.44	m	5.60	m
12-CH_3	1.66	dt; 6, 1.5	1.70	d; 5.8
7-OCH_3	3.78	s	3.84	s

[a] For numbering of TME refer to Figure 1. [b] All chemical shifts are given in parts per million relative to tetramethylsilane (Me_4Si). [c] Abbreviations: dd, doublet of doublets; bd, broad doublet; bs, broad singlet; s, singlet; d, doublet; m, multiplet; td, triplet of doublets; dt, doublet of triplets. [d] Signal buried under signals at 4.28 ppm.

X-ray structure (Arora, 1981; Tozuka & Takaya, 1983). However, the 11*S*,11a*S* diastereomer appears to adopt a different conformation. Using the coupling information in conjunction with Karplus rule, it was possible to construct a stereomodel that agreed with the data. The 11*S*,11a*S* form of TME has a slightly greater twist along the length of the molecule than the 11*R*,11a*S* form, and significantly, the carbonyl is displaced out of planarity with the aromatic ring to a greater extent than in the 11*R*,11a*S* form. This explains the differences in the resonances for the H-3 protons of the two diastereomers. In the 11*R*,11a*S* form the H-3 protons are degenerate and are deshielded by the carbonyl to 4.25 ppm. Inspection of stereomodels reveals that each proton is approximately equidistant from the carbonyl. On the other hand, in the 11*S*,11a*S* form one of these protons is shifted upfield to 4.06 ppm. The stereomodel indicates that the carbonyl is more distant from H-3b than from H-3a, accounting for the observed upfield shift. Other shifts such as the upfield shift of H-6 in the 11*S*,11a*S* form can be similarly rationalized.

(*2*) *Fluorescence Studies.* The fluorescence decay of tomaymycin is biexponential in protic solvents and on DNA (see below). The two emitting species represent two fluorescent ground-state forms with closely overlapped spectra and different excited-state lifetimes. This is manifest in the wavelength dependence of the steady-state spectra and fluorescence quantum yield. Figure 4A shows the absorption spectrum of TME equilibrated in methanol (broken line); the long-wavelength maximum is at about 320 nm (Arima et al., 1972). The fluorescence emission maximum is at about 400 nm, or about 20 nm to the red compared to acetonitrile. The emission and excitation maxima depend on excitation and emission wavelength. Figure 5A shows the emission spectra of TME in methanol corresponding to excitation at half-maximal absorption on either side of the 320-nm band. Excitation on the red (342 nm) shifts the emission spectra about 5 nm to the blue compared to excitation on the blue (296 nm). The excitation spectra show corresponding spectral shifts (data not shown). Thus, there are at least two absorbing and emitting species with different but overlapping spectra: the species that absorbs on the red emits on the blue, whereas the species that absorbs on the blue emits on the red. Furthermore, the apparent quantum yield of TME in methanol increases with increasing excitation wavelength (Table I). In principle, the quantum yield of a pure compound should be independent of excitation wavelength. The wavelength dependence of the apparent quantum yield indicates that there is more than one absorbing species. If it were due entirely to the presence of a nonfluorescent compound, then the steady-state spectra would be independent of wavelength. The increase in quantum yield with excitation wavelength indicates that the species that

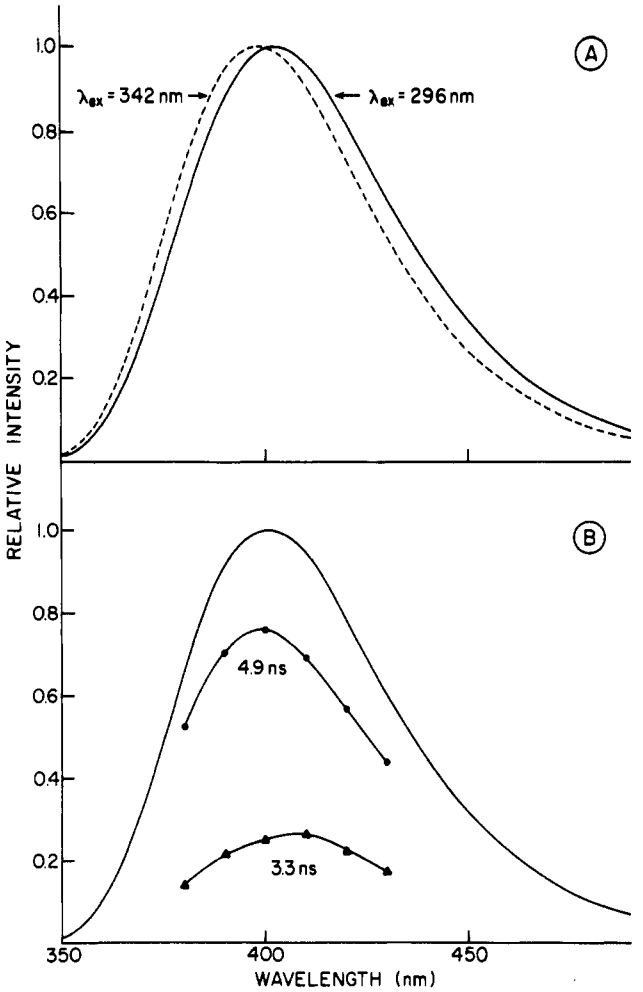

FIGURE 5: Fluorescence emission spectra of TME in methanol. (A) Corrected steady-state emission spectra at different excitation wavelengths: (—) λ_{ex} = 296 nm; (---) λ_{ex} = 342 nm. Spectra are normalized to the peak. (B) Decay-associated emission spectra: (—) corrected steady-state spectrum at λ_{ex} = 313 nm; (●) 4.9- and (▲) 3.3-ns components scaled to the steady-state spectrum. Lines were drawn to connect the points.

absorbs on the red contributes an increasing fraction of the total emission.

The time-resolved fluorescence data extend the conclusions based on steady-state measurements. The fluorescence decay of TME in methanol is adequately described by a biexponential function with lifetimes of 3.3 and 4.9 ns and positive amplitudes that depend on excitation and emission wavelength (Table II). Because accurate resolution of such closely spaced decays (lifetimes differing by less than a factor of 2) is generally not possible from analysis of single decay curves, the data presented in Table II were obtained from global analyses of multiple decay curves collected at different wavelengths (Knutson et al., 1983). Fluorescence decays of TME in methanol were measured for six emission wavelengths (380–430 nm, 10-nm increments) at both 313- and 337-nm excitation. The 12 decay curves were analyzed by a global least-squares fitting program: the global χ_r^2 = 1.4 for two exponentials compared to χ_r^2 = 3.5 for a single exponential. No significant improvement in fit was obtained for three exponentials. As seen in Table II, the amplitude α_1 of the 3.3-ns decay decreases and the amplitude α_2 of the 4.9-ns decay increases as the excitation wavelength is increased. The changes in the relative amplitudes with excitation wavelength at constant emission wavelength are due only to differences in the absorption spectra of the two lifetime components. Thus, the 4.9-ns component absorbs to the red of the 3.3-ns component. This is illustrated in Figure 4B, which shows the decay-associated excitation spectra of the two components normalized to the long-wavelength peak. The excitation maximum is at about 328 nm for the 4.9-ns component compared to 320 nm for the 3.3-ns component. The decay-associated emission spectra of the two components are depicted in Figure 5B. The emission maximum of the 4.9-ns component lies about 10 nm to the blue of the peak of the 3.3-ns component. The 4.9-ns decay contributes about 75% of the fluorescence intensity at 313-nm excitation.

The fluorescence properties of MTME in methanol are similar to those of TME, with minor quantitative differences (Tables I and II).

(3) Correlation of ^{1}H NMR and Fluorescence Results. The ^{1}H NMR studies enable us to identify the two fluorescent ground-state forms of tomaymycin in methanol. According to the ^{1}H NMR, the 11*R*,11a*S* diastereomer is present in about 65:35 excess of the 11*S*,11a*S* diastereomer at equilibrium. Moreover, the two diastereomers adopt different conformations in methanol, which accounts for the absorption spectral shifts. We can make a crude estimate of the relative concentrations of the two ground-state species from the amplitudes α_1 and α_2 of the fluorescence decay. The relative amplitude α_i of component i depends on several factors

$$\alpha_i(\lambda_{ex},\lambda_{em}) = \epsilon_i(\lambda_{ex})I_i(\lambda_{em})k_{R,i}c_i$$

including its molar extinction spectrum ϵ_i, emission spectrum I_i, radiative rate constant $k_{R,i}$, and concentration c_i. Assuming that the radiative rates of the two species are similar, the relative extinction coefficients $\epsilon_i(\lambda_{ex})$ may be estimated from the normalized decay-associated excitation spectra in Figure 4B. The relative fluorescence $I_i(\lambda_{em})$ may be estimated after normalization of the decay-associated emission spectra in Figure 5B. Using the amplitudes in Table II, we find the relative concentrations of the 4.9- and 3.3-ns components to be roughly 75:25. Thus, the longer lifetime component present in excess must be the 11*R*,11a*S* diastereomer, and the shorter lifetime component must be the 11*S*,11a*S* diastereomer. Furthermore, the longer lifetime component has its absorption band on the red compared to the shorter lifetime component. The ^{1}H NMR conformational analysis indicates that the C-5 carbonyl lies closer to the plane of the aromatic ring in the 11*R*,11a*S* diastereomer. The more extensive conjugation possible in the 11*R*,11a*S* diastereomer would shift the $\pi \rightarrow \pi^*$ transition to lower energy. At present we are unable to explain the difference in observed lifetimes of the two diastereomers in methanol or of the 11*R*,11a*S* diastereomer in different solvents (methanol vs. acetonitrile). We note that the extinction coefficient of tomaymycin, which is typical of a weak $\pi \rightarrow \pi^*$ transition, is essentially independent of environment (Table I). This implies that the radiative rates do not vary much, so that other processes that compete for deactivation of the excited state must govern the differences in observed lifetimes.

The assignment of the longer lifetime species that absorbs on the red to the 11*R*,11a*S* diastereomer, and of the shorter lifetime species that absorbs on the blue to the 11*S*,11a*S* diastereomer, was confirmed by monitoring the time course of epimerization by ^{1}H NMR, absorbance, and fluorescence. The ^{1}H NMR shows only the 11*R*,11a*S* diastereomer immediately after dissolution of TME in methanol (Figure 2C). The relative amounts of the 11*R*,11a*S* and 11*S*,11a*S* forms are about 8:1 after 0.5 h and 4:1 after 1 h. Figure 4A shows the absorption spectra of TME at various times after dissolving the crystals in methanol. The peak is at about 325 nm after

0.5 h and shifts about 5 nm to the blue in 3–4 h, with isosbestic points at 315, 279, and 263 nm. The isosbestic points signify two ground-state species. The absorption spectral changes correlated as expected with changes in the amplitudes of the fluorescence decay: the amplitude α_2 of the 4.9-ns decay decreased while the amplitude of the 3.3-ns decay increased with time. At 313-nm excitation and 405-nm emission, 89% of the fluorescence intensity arises from the 4.9-ns component after about 1 h, compared to 73% at equilibrium.

Fluorescence of Tomaymycin in Aqueous Solution and on DNA. In aqueous solution TME is presumably hydrolyzed to the carbinolamine. The carbinolamine in pH 5 buffer has an absorption spectrum similar to TME in methanol, but with a peak at 310 nm (Table I). The fluorescence emission maximum is at about 410 nm. The carbinolamine occurs in one major fluorescent ground-state form of lifetime 1.1 ns, with a trace of a second longer lifetime species. The fluorescence decay gives an acceptable fit (global $\chi_r^2 = 1.6$) to a monoexponential function. However, a somewhat better fit (global $\chi_r^2 = 1.4$) is always obtained by including a minor second component (Table II). Because this component comprises only about 1% of the fluorescence intensity, the longer lifetime is not accurately determined. The second component is more visible in the fluorescence decay of the 8-*O*-methyl derivative. In this case, the fit to a biexponential function (global $\chi_r^2 = 1.2$) is significantly improved compared to the fit to a monoexponential (global $\chi_r^2 = 27$). A small decrease in amplitude α_1 of the major 1.3-ns decay and an increase in amplitude α_2 of the minor 8-ns decay with increasing excitation wavelength are also detectable. The presence of a second fluorescent ground-state form is supported by a slight wavelength dependence of the steady-state spectra and quantum yield (Table I). The excitation and emission spectral shifts and the increase in quantum yield with excitation wavelength are similar to but smaller than those observed for TME and MTME in methanol. Since identical results were obtained for solutions prepared after repeated evaporation of aqueous solutions of the 11-methyl ethers, it is likely that the minor species is carbinolamine and not unhydrolyzed 11-methyl ether. The spectral characteristics of the carbinolamine, which absorbs to the blue and emits to the red of the methyl ether in acetonitrile and methanol, suggest that it is mainly the 11*S*,11a*S* diastereomer. This conclusion is substantiated by ^{1}H NMR (Cheatham and Hurley, unpublished results). The minor longer lifetime species, which accounts for the small increase in quantum yield with excitation wavelength, would then be the 11*R*,11a*S* diastereomer of the carbinolamine.

As already mentioned, there are two fluorescent ground-state forms of tomaymycin in the calf thymus DNA adduct. The long-wavelength absorption band of the adduct is typical of tomaymycin in other solvents, but the maximum is red-shifted to about 330 nm (Table I). The steady-state emission spectrum is almost independent of excitation wavelength with a maximum at about 405 nm, though the fluorescence quantum yield increases with increasing excitation wavelength. The fluorescence decay of the tomaymycin–DNA adduct gives a good fit (global $\chi_r^2 = 1.3$) to a biexponential function with lifetimes of 3.0 and 5.5 ns (Table II). No improvement in the fit is obtained for three exponentials. Time-resolved emission spectroscopy shows that the emission spectra of the two components are almost identical (Barkley, Thomas, and Maskos, unpublished results), in agreement with the steady-state results. However, fluorescence decay measurements at three excitation wavelengths indicate that the absorption spectra of the two species are slightly different. As seen in Table II, the amplitude of the 5.5-ns component increases, whereas the amplitude of the 3.0-ns component decreases, with increasing excitation wavelength. Thus for the tomaymycin–DNA adduct, as well as the free drug in protic solvents, the longer lifetime species is associated with an absorption band on the red, and the shorter lifetime species is associated with an absorption band on the blue. The longer lifetime species contributes about 80% of the fluorescence intensity. The possibility that the fluorescence results are influenced by residual unreacted tomaymycin even at low binding density (phosphate/drug = 125 in all experiments) is excluded by two observations. First, the time-resolved data show no evidence for a third component. Second, the decay parameters are not affected by extraction of the DNA adduct with isobutanol to remove unreacted drug, followed by ether to remove the alcohol. The latter result also demonstrates that neither fluorescent species is a noncovalently bound form of tomaymycin. Since the 8-*O*-methyltomaymycin–DNA adduct has similar fluorescence properties (Tables I and II), the two fluorescent species cannot be due to proton-transfer reactions in the ground and/or excited state, which involve the 8-phenolic proton. This titratable proton in tomaymycin has a $pK_a = 8.0$, and the anion has very weak fluorescence (Barkley, Thomas, and Maskos, unpublished results). Proton-transfer reactions of the N-10 proton are possible but unlikely.

The ^{1}H NMR and fluorescence results for tomaymycin in protic solvents suggest a plausible explanation for the two fluorescent ground-state forms of the DNA adduct, namely, that the two emitting species represent the two diastereomeric forms of tomaymycin bound to DNA. The alternative explanation would be that the heterogeneous emission arises from a single diastereomer bound in different environments on DNA. For the reasons discussed later, we favor the former interpretation and carried out molecular modeling studies to test this proposal.

Molecular Modeling Studies. In order to assess the feasibility of binding the 11*R*,11a*S* and 11*S*,11a*S* diastereomers of tomaymycin to DNA, molecular modeling studies were conducted. CPK model building studies showed that tomaymycin in the conformation *associated* with the 11*R*,11a*S* diastereomer of TME could be bound covalently to DNA through N-2 of guanine with minimal steric interactions, providing the 11*S* linkage geometry was used. Conversely, in order to dock tomaymycin to DNA via an 11*R* linkage, it is necessary to use the conformation *associated* with the 11*S*,11a*S* diastereomer of TME. Superficially, this might suggest that when tomaymycin binds to DNA it undergoes a net inversion of configuration at C-11. However, as described later, we favor a binding mechanism that involves attack by N-2 of guanine on the reactive N-10,C-11 imine (Scheme I). Since in principle the imine could be produced by loss of water from either the 11*R*,11a*S* or 11*S*,11a*S* carbinolamine of tomaymycin, the mechanism should not be considered in terms of retention or inversion of configuration. As a direct consequence of binding via the 11*S* or 11*R* configuration, the tomaymycin molecules will lie in opposite orientations in the minor groove of DNA: tomaymycin attached by an 11*S* linkage is oriented with the aromatic ring on the 3′ side of the covalently modified guanine, whereas tomaymycin attached by an 11*R* linkage is oriented with the aromatic ring on the 5′ side. The results of molecular graphics modeling studies with tomaymycin and the 6-mer duplex $d(ATGCAT)_2$ are shown in Figure 6. These stereo diagrams of the tomaymycin–$d(ATGCAT)_2$ adduct were generated by using the all-atom force field parameters of Amber. A full account of these

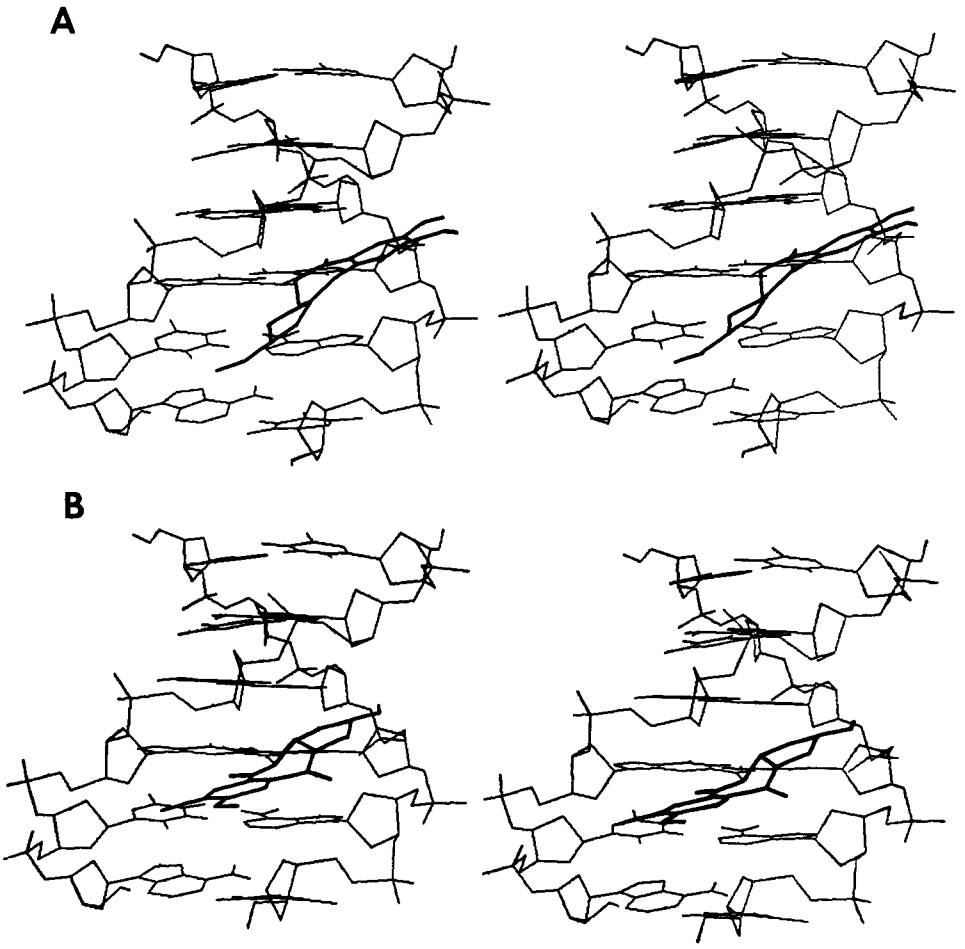

FIGURE 6: Stereo diagrams of (A) the (11*S*,11a*S*)-tomaymycin–d(ATGCAT)$_2$ duplex and (B) the (11*R*,11a*S*)-tomaymycin–d(ATGCAT)$_2$ duplex adducts.

energy analyses will be published later (Remers et al., 1986).

Discussion

The ^{1}H NMR and fluorescence studies on tomaymycin provide excellent evidence for the following conclusions: (1) While TME crystallizes from methanol as the 11*R*,11a*S* diastereomer, when dissolved in chloroform it loses methanol to form the 10,11-anhydrotomaymycin, and when dissolved in methanol it equilibrates to about a 65:35 mixture of the 11*R*,11a*S* and 11*S*,11a*S* diastereomers.[3] (2) By analogy with the fluorescence properties of tomaymycin in protic solvents, two conformational forms of tomaymycin are bound covalently to DNA. (3) In buffer at pH 5.1 the predominant form of tomaymycin is the shorter lifetime species which absorbs on the blue (presumably the 11*S*,11a*S* diastereomer), while on DNA the major form is the longer lifetime species which absorbs on the red (presumably the 11*R*,11a*S* conformational form attached by the 11*S* linkage). (4) Molecular modeling studies show that both the 11*R*,11a*S* and 11*S*,11a*S* diastereomers can bind to the 6-mer duplex of 5′ATGCAT without appreciable steric hindrance.

Although tomaymycin like other members of the P[1,4]B antibiotic group reacts only at guanine residues (Petrusek et al., 1981), the environment of the drug on natural DNA sequences will be heterogeneous. Thus, the fluorescence emission is understandably heterogeneous. A number of acridine dyes exhibit multiexponential fluorescence decays when bound to DNA but single-exponential decays when free in solution (Kuboto & Motuda, 1980; Barkley et al., 1981; Kubota et al., 1984). The heterogeneous emission of these intercalating dye–DNA complexes has been attributed to sequence-dependent quenching processes and alternative binding modes (Kubota & Motuda, 1980; Kubota et al., 1984). In contrast, tomaymycin fluorescence is heterogeneous in both homogeneous and heterogeneous environments. It is tempting to speculate that the same mechanism produces the ground-state heterogeneity in both cases. If so, the two fluorescent ground-state forms of tomaymycin bound to DNA should represent two diastereomeric forms of the DNA adduct. Molecular mechanics and ^{1}H NMR studies on drug–oligodeoxynucleotide adducts (see below) provide additional evidence that two diastereomeric forms of tomaymycin can bind to DNA containing heterogeneous sequence environments. Another explanation for the ground-state heterogeneity would be a single diastereomeric form bound at different DNA sites. There would undoubtedly be a distribution of such sites, corresponding to various sequences around the covalently attached guanine. If each type of environment resulted in a somewhat different lifetime, then the fluorescence decay might appear to be biexponential. In either mechanism, the absorption spectral shifts presumably reflect different conformations of the covalently bound drug.

Primarily on the basis of CPK model building studies with anthramycin, tomaymycin, sibiromycin, and the neothramycins, we had previously assigned the stereochemistry at the covalent DNA linkage site as *S* (Petrusek et al., 1981).

[3] In a previous paper (Petrusek et al., 1981) the stereochemistry at C-11a is represented in the figure correctly but erroneously assigned the absolute configuration *R* in the text.

As noted above, the stereochemistry at the linkage site of the adduct dictates the orientation of the P[1,4]B nucleus in the minor groove of DNA. If the linkage geometry is *S*, then the aromatic ring of the *P*[1,4]B's lies to the 3′ side of the covalently modified guanine. For the anthramycin–d(ATGCAT)$_2$ adduct this assignment has been confirmed by using 2-D ^{1}H NMR techniques (Graves et al., 1985). We have recently examined the tomaymycin–d(ATGCAT)$_2$ adduct by ^{1}H NMR and observed a mixed orientation on DNA with approximately equal amounts of the 11*R*,11a*S* and 11*S*,11a*S* diastereomeric adducts (Cheatham and Hurley, unpublished results). Remers et al. (1986) have predicted energy differences between the two diastereomeric forms of these duplex adducts using the molecular mechanics program Amber, which agree with the ^{1}H NMR results. They calculate −10.8 kcal/mol difference between the 11*S*,11a*S* and 11*R*,11a*S* diastereomers for anthramycin bound to d(ATGCAT)$_2$ compared to only a −2.3 kcal/mol difference for tomaymycin. In both cases the 11*S*,11a*S* adduct was more stable than the 11*R*,11a*S* adduct. At least two structural factors may be responsible for the more restricted orientation of anthramycin on DNA. First, the 2,3-unsaturated pyrrolo ring imparts a steeper twist to the anthramycin molecule (35°) than the pyrrolo exocyclic double bond in tomaymycin (7°). This constraint, coupled with the presence of a 9-phenolic group on the aromatic ring of anthramycin, appears to impart a steric hindrance to binding through an 11*R* linkage to DNA.

Sequence specificity studies with tomaymycin and related drugs demonstrate that 5′PuGPu sequences are preferred binding sites for the P[1,4]B's (Hertzberg et al., 1986). Nevertheless, other sequences such as the least preferred 5′PyGPy sequence will bind tomaymycin, although these sites are kinetically less favored. It seems reasonable to expect that the 5′PuGPu sites may show less orientational ambiguity in binding tomaymycin than the 5′ATGCAT sequence. Furthermore, it is possible that there are as yet undefined sequences that bind tomaymycin as either the 11*S*,11a*S* or 11*R*,11a*S* diastereomeric adduct. In this regard, fluorescence measurements show that only the longer lifetime component binds to poly(dG-dC) (Barkley, Thomas, and Maskos, unpublished results).

Since the relative amounts of the two forms of tomaymycin on DNA do not appear to correspond to the relative amounts existing in buffer (Table II), a simple relationship whereby the proportions of bound tomaymycin species depend upon the relative amounts of free diastereomers can be discounted. More likely, the relative affinities and frequency of occurrence of different binding sequences for the DNA-reactive tomaymycin species in large part determine the proportions of the two forms of tomaymycin bound to DNA. The facile conversion of the two diastereomers of TME via the 10,11-anhydrotomaymycin suggests that the relatively planar imine may be the ultimate DNA-reactive compound (Hurley, 1977; Lown & Joshua, 1979). Consequently, the orientation of the reactive tomaymycin compound in the minor groove and the proximity of an appropriate sequence will determine whether the drug molecule binds to produce an 11*S* or 11*R* diastereomeric DNA adduct.

The sequence-specific orientation of P[1,4]B's in the minor groove of DNA and those inherent structural factors that can influence the orientation of a particular drug molecule are important considerations in drug design. The synthesis of analogues of naturally occurring P[1,4]B antibiotics that will either reveal or direct their orientation in the minor groove is in progress. The availability of such orientation-specific molecules will allow us to continue our drug development work and provide specific fluorescent probes to monitor internal motions in DNA.

ACKNOWLEDGMENTS

We are most grateful to Dr. William Remers at the University of Arizona for permission to use his unpublished data on molecular modeling studies on the tomaymycin–d(ATGCAT)$_2$ adduct. Figure 6 was generously provided by Dr. Remers. We thank Dr. Thomas Krugh for providing unpublished data on the ^{1}H NMR of the anthramycin–d(ATGCAT)$_2$ adduct and Dr. Alan Kook for obtaining the 2-D COSY results on TME. We also thank Dr. Ludwig Brand and Joseph Beechem for advice on the global deconvolution program, Dr. Jay Knutson for providing the indirect method for decay-associated excitation spectra, and Dr. Zbigniew Kolber for assistance with fluorescence decay measurements. Dr. Bernard Zietek participated in the preliminary studies that led to this work. Finally, we acknowledge the skill and patience of Lesley Koop in preparation of the manuscript.

Registry No. d(ATGCAT), 101226-07-7; 10,11-anhydrotomaymycin, 81422-30-2; Figure 1, R^1 = R^2 = Me, 89300-14-1; Figure 1, R^1 = Me, R^2 = H (11*R*,11a*S*), 35050-55-6; Figure 1, R^1 = Me, R^2 = H (11*S*,11a*S*), 101313-08-0.

REFERENCES

Arima, K., Kohsaka, M., Tamura, G., Imanaka, H., & Sakai, H. (1972) *J. Antibiot. 24*, 437–444.

Arora, S. (1981) *J. Antibiot. 34*, 462–464.

Barkley, M. D., Kowalczyk, A. A., & Brand, L. (1981) *J. Chem. Phys. 75*, 3581–3593.

Bevington, P. R. (1969) *Data Reduction and Error Analysis for the Physical Sciences*, McGraw-Hill, New York.

Graves, D. E., Pattaroni, C., Krishnan, B. S., Ostrander, J. M., Hurley, L. H., & Krugh, T. R. (1984) *J. Biol. Chem. 259*, 8202–8209.

Graves, D. E., Stone, M. P., & Krugh, T. R. (1985) *Biochemistry 24*, 7573–7581.

Grinvald, A., & Steinberg, I. Z. (1974) *Anal. Biochem. 59*, 583–598.

Hertzberg, R. P., Hecht, S. M., Reynolds, V. L., Molineux, I. J., & Hurley, L. H. (1986) *Biochemistry 25*, 1249–1258.

Hurley, L. H. (1977) *J. Antibiot. 30*, 349–370.

Hurley, L. H. (1980) *Acc. Chem. Res. 13*, 263–269.

Hurley, L. H., & Thurston, D. E. (1984) *Pharm. Res. 1*, 51–59.

Hurley, L. H., Gairola, C., & Zmijewski, M. (1977) *Biochim. Biophys. Acta 475*, 521–535.

Kariyone, K., Yazawa, H., & Kohsaka, M. (1971) *Chem. Pharm. Bull. 19*, 2289–2293.

Karplus, M. (1959) *J. Chem. Phys. 30*, 11–15.

Knutson, J. R., Beechem, J. M., & Brand, L. (1983) *Chem. Phys. Lett. 102*, 501–507.

Kolber, Z. S., & Barkley, M. D. (1986) *Anal. Biochem. 152*, 6–21.

Kubota, Y., & Motoda, Y. (1980) *Biochemistry 19*, 4189–4197.

Kubota, Y., Motoda, Y., Kuromi, Y., & Fujisake, Y. (1984) *Biophys. Chem. 19*, 25–37.

Leimgruber, W., Stefanovic, V., Schenker, F., Karr, A., & Berger, J. (1965) *J. Am. Chem. Soc. 87*, 5791–5793.

Lown, J. W., & Joshua, A. V. (1979) *Biochem. Pharmacol. 28*, 2017–2026.

Maruyama, I. N., Suzuki, H., & Tanaka, N. (1978) *J. Antibiot. 31*, 761–768.

Melhuish, W. H. (1961) *J. Phys. Chem. 65*, 229–235.

Petrusek, R. L., Anderson, G. L., Garner, T. F., Quinton, F. L., Fannin, L., Kaplan, D. J., Zimmer, S. G., & Hurley, L. H. (1981) *Biochemistry 20*, 1111–1119.
Remers, W. A., Mabilia, M., & Hopfinger, A. G. (1986) *J. Med. Chem.* (submitted for publication).
Thurston, D. E., & Hurley, L. H. (1984) *Drugs Future 8*, 957–971.
Tozuka, Z., & Takaya, T. (1983) *J. Antibiot. 36*, 142–146.
Tozuka, Z., Takasugi, H., & Takaya, T. (1983) *J. Antibiot. 36*, 276–282.

Modulation of Platinum Antitumor Drug Binding to DNA by Linked and Free Intercalators†

Bruce E. Bowler and Stephen J. Lippard*
Department of Chemistry, Massachusetts Institute of Technology, Cambridge, Massachusetts 02139
Received October 18, 1985; Revised Manuscript Received January 2, 1986

ABSTRACT: We report the DNA binding site preferences of the novel molecule AO–Pt, in which the anticancer drug dichloro(ethylenediamine)platinum(II) is linked by a hexamethylene chain to acridine orange. The sequence specificity of platinum binding was mapped by exonuclease III digestion of 165 and 335 base pair restriction fragments from pBR322 DNA. Parallel studies were carried out with the unmodified anticancer drugs *cis*-diamminedichloroplatinum(II) (*cis*-DDP) and dichloro(ethylenediamine)platinum(II), [Pt(en)Cl_2]. Oligo(dG) sequences are the most prevalent binding sites for AO–Pt, with secondary binding occurring mainly at d(AG) sites. *cis*-DDP and [Pt(en)Cl_2] bind less readily to the secondary sequences, with *cis*-DDP showing greater binding site selectivity than [Pt(en)Cl_2]. The DNA intercalator ethidium bromide promotes binding of [Pt(en)Cl_2] and *cis*-DDP to many sites containing d(CGG) and, to a lesser extent, d(AG) sequences. AO–Pt exhibits enhanced binding to these sequences without the need for an external intercalator. Unlinked acridine orange, however, does not promote binding of [Pt(en)Cl_2] and *cis*-DDP to d(CGG) and d(AG) sequences. These results are discussed in terms of the sequence preferences, stereochemistry, and relative residence times of the intercalators at their DNA binding sites. By modulating local structure in a sequence-dependent manner, both linked and, in the case of ethidium, free intercalators can influence the regioselectivity of covalent modification of DNA by platinum antitumor drugs.

There is currently much interest in understanding the interaction of platinum complexes with DNA (Pinto & Lippard, 1985; Hacker et al., 1984). This attention stems mainly from the clinical success of *cis*-diamminedichloroplatinum(II), *cis*-DDP,[1] in the treatment of neoplastic disease, particularly testicular cancer (Prestayko et al., 1980; Loehrer & Einhorn, 1984), as well as evidence pointing to differential repair of Pt–DNA adducts as an important aspect of the molecular mechanism of action of the drug (Roberts & Pera, 1983; Ciccarelli et al., 1985). Numerous in vitro and in vivo studies have elucidated both the sequence specificity and structural changes coincident with platinum binding to DNA (Pinto & Lippard, 1985).

In most of this work, platinum–DNA interactions have been studied in the absence of other perturbing agents in the medium. Since *cis*-DDP is usually administered in combination with other drugs, such as actinomycin, vinblastine, bleomycin, and adriamycin (Pizzocaro et al., 1985; Loehrer & Einhorn, 1984; Vugrin et al., 1983; Prestayko et al., 1980), several of which are DNA intercalators [Berman & Young (1981) and references cited therein], we were interested to monitor the mutual effects of DNA intercalators and platinum complexes on DNA binding. Previously, we showed that *cis*-DDP alters the sequence-specific cleavage of DNA by bleomycin (Mascharak et al., 1983) and that the intercalator EthBr changes both the position (Tullius & Lippard, 1982) and the mode (Merkel & Lippard, 1982) of *cis*-DDP binding to DNA. Since these modulations might be related to the clinical synergism between *cis*-DDP and an intercalating antitumor drug, we have extended our investigation to gain further insight into the important parameters involved in the alteration of DNA–platinum binding by DNA intercalators. Specifically, we have synthesized a platinum complex, AO–Pt (Bowler et al., 1984), that covalently links [Pt(en)Cl_2] to the DNA intercalator AO by a polymethylene chain (Figure 1). This compound permits local modifications of DNA structure by an intercalator to be sampled by platinum without the need to add a large excess of external intercalator. Thus, the effect of the intercalator can be monitored at low $(D/N)_0$ ratios of both platinum and intercalator. This approach of coupling metals with DNA intercalators has been used in previous studies involving metallointercalators (Lippard, 1978; Barton, 1983) and intercalator-linked iron complexes (Van Dyke & Dervan, 1984;

† This work was supported by U.S. Public Health Service Grant CA-34992 from the National Cancer Institute. B.E.B. acknowledges the Canadian Natural Sciences and Engineering Research Council for a postgraduate scholarship.

[1] Abbreviations: EthBr, ethidium bromide; AO, acridine orange; CIP, calf intestinal phosphatase; PNK, T4 polynucleotide kinase; Tris, tris(hydroxymethyl)aminomethane; EDTA, ethylenediaminetetraacetate; DTT, dithiothreitol; bp, base pair; β-ME, β-mercaptoethanol; $(D/N)_0$, added drug to nucleotide ratio; $(D/N)_b$, bound drug to nucleotide ratio; *cis*-DDP, *cis*-diamminedichloroplatinum(II); en, ethylenediamine; pur, purine; pyr, pyrimidine; AO–Pt, the intercalator-linked (ethylenediamine)platinum(II) complex; AO-en, 3,6-bis(dimethylamino)-10-[6-[(2-aminoethyl)amino]hexyl]acridinium chloride.

0006-2960/86/0425-3031$01.50/0